Construction and Building Materials 229 (2019) 116875

Contents lists available at ScienceDirect

Construction and Building Materials

journal homepage: www.elsevier.com/locate/conbuildmat

Quantification of residual cement paste on recycled concrete aggregates containing limestone by selective dissolution

Rafael dos Santos Macedo [a,*], Carina Ulsen [a], Anette Mueller [b]

[a] Department of Mining and Petroleum Engineering, Polytechnic School, University of Sao Paulo – Technological Characterization Laboratory, Brazil
[b] Weimar Institute of Applied Construction Research, Germany

HIGHLIGHTS

- Quantification of cement paste in recycled aggregates by calcium leaching.
- The dissolution method is selective despite the presence of carbonates.
- The method has good correlation between the real and estimated cement content.

GRAPHICAL ABSTRACT

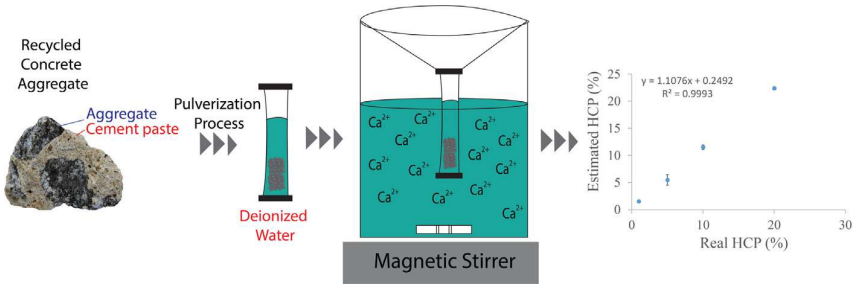

ARTICLE INFO

Article history:
Received 14 May 2019
Received in revised form 9 July 2019
Accepted 2 September 2019
Available online 12 September 2019

Keywords:
Construction and demolition wastes
Cement paste
Recycled concrete
Selective dissolution

ABSTRACT

This study proposes a new method of selective dissolution of calcium from C-S-H and CH phases by deionized water to evaluate the cement paste content in recycled concrete aggregates (RCA). The selective dissolution tests were carried out in standard phases of hydrated cement paste (HCP), calcite, dolomite and quartzite sand, and mixtures simulating RCA containing 1,5,10,20% HCP. The materials were characterized by X-ray diffractometry, thermal analysis, Raman and infrared spectroscopic analyzes, chemical analysis and laser diffraction analysis. Materials characterization indicates good selectivity of the deionized water in the calcium dissolution of the CH and C-S-H compared to limestone.

1. Introduction

Construction and demolition waste (CDW) consists of a set of materials arrive from constructions, restorations and demolitions [1]. The construction and demolition, mining and quarrying operation activities of European Union contains more than 90% of mineral phases [2]. The chemical composition of the CDW depends on the intrinsic characteristics of each construction; the components generally include concrete, metals, gypsum, asphalt, soil, masonry blocks (red or calcium silica bricks) and other materials [3–5].

Concrete is one of the most commonly found materials in recycled aggregates (RA)[3], consisting mainly of coarse and fine aggregates, water and binder materials (Portland cement and composite cement) [6,7]. About 60–75% of the total concrete volume consists of mineral aggregates. Therefore, the high mineral content in concrete associated with the environmental impact of the consumption and exploitation of natural aggregates (NA) for constructions, motivate the use of recycled concrete aggregates (RCA) in order to strengthen the concept of circular mining [2].

The positive aspects of RCA reuse are unequivocal in the quest for sustainability of the construction industry materials, but there

* Corresponding author at: Department of Mining and Petroleum Engineering, Polytechnic School, University of Sao Paulo, Av. Prof. Mello Moraes, 2373, Butantã, CEP 05508-030, São Paulo, SP, Brazil.
E-mail address: rafaelmacedo@usp.br (R. dos Santos Macedo).

https://doi.org/10.1016/j.conbuildmat.2019.116875
0950-0618/

are still some difficulties associated with the use of RCA in civil construction. The main issue about RCA applications concern to the lack of specifications and standards in the production of RCA, consequently affects the reliability of the product in the market [2].

The composition of the natural aggregates derives from the geological sites of the rocks, presenting distinct properties as the chemical and mineralogical composition, density, porosity and others. Some examples of minerals found in NA used in the manufacture of concrete are mostly represented by quartz (SiO_2), feldspars ($KAlSi_3O_8$), calcite ($CaCO_3$), and other commonly used NA in minor quantities are muscovite ($KAl_2[AlSi_3O_{10}](OH)_2$), dolomite ($Ca_{1-x}Mg_xCO_3$), biotite ($K(Mg,Fe)_3AlSi_3O_{10}(OH)_2$), gypsum ($CaSO_4 \cdot 2H_2O$), pyrite ($FeS_2$), clays $(Na,Ca)_{0.33}(Al,Mg)_2(Si_4O_{10})(OH)_2 \cdot nH_2O$,) and hematite ($Fe_2O_3$) [8].

According to Taylor (1997) [6], Portland cement is composed of a mixture, basically clinker, a minor percent of calcium sulphate and finely ground. The clinker typically has a composition in the region of 67% CaO, 22% SiO_2, 5% Al_2O_3, 3% Fe_2O_3 and 3% other components, and normally contains four major phases, alite (C_3S; (50–70%)), belite (C_2S; (15–30%)), aluminate (C_3A; (5–10%)) and ferrite (C_2F; (5–15%)). The main clinker components, alite, belite, aluminate and ferrite are partially hydrated. Alite and belite hydration produce the C-S-H and portlandite phases ($CH{=}Ca(OH)_2$) (Eq. 1–4). The aluminates and ferrites have numerous hydrated phases, a relevant example in the presence of sulfates that occupies a considerable volume in the hydrated cement is the ettringite (AFT) (Eq. 5 and 6) [9–11].

$$\text{Alite} + 6(CaO) \cdot 2(SiO_2) + 11H_2O \rightarrow 3(CaO) \cdot 2(SiO_2) \cdot 8(H_2O) + 3(Ca(OH)_2) \quad (1)$$

$$2C_3S + 11H \rightarrow C_3S_2H_8 + 3CH \quad (2)$$

$$\text{Belite} + 4(CaO) \cdot 2(SiO_2) + 9H_2O \rightarrow 3(CaO) \cdot 2(SiO_2) \cdot 8(H_2O) + Ca(OH)_2 \quad (3)$$

$$2C_2S + 9H \rightarrow C_3S_2H_8 + 3CH \quad (4)$$

$$\text{Aluminate} + Ca_3Al_2O_6 + 3(CaSO_4 \cdot 2H_2O) + 26H_2O \rightarrow Ca_6Al_2(SO_4)_3(OH)_{12} \cdot 26H_2O \quad (5)$$

$$C_3A + 3\left(C\bar{S}H_2\right) + 26H \rightarrow AFt \quad (6)$$

At the moment, the methods applied to certify the RCA quality are the same as those used for NA [12], however, there are substantial differences in the chemical composition, texture and densities of these materials. The main factors that impact the quality of the RCA are heterogeneities of the materials in the source extraction and the remnant cement paste content.

The method of water absorption is one of the indirect methods used to evaluate the content of cement paste in RCA, since the porosity of the RCA is derived mostly from the cement paste [13]. The methods employed are standardized for coarse (ASTM C127-15) [14] and fine (ASTM C128-15) [15] natural aggregates. These methods are used also for RCA, however, during the experiments with RCA researchers report weight loss of 2–9 times greater when compared to tests performed with natural aggregates, according to the literature this occurrence is related to particle disintegration and fine particle retention during the experiment [16,17].

Other alternative methods for cement paste quantification in RCA already been developed such as, microscopy by image analysis [18], thermal treatment [19,20] and chemical attack by acid leaching [5,19,21]. The pursuit for an efficient method for quantifying the cement paste content is linked to the ability to apply chemical substances or develop techniques capable of responding differently for mineral and cement paste phases.

Table 1
Some hydroxides and mineral phases $\log_{10}$ K_{sp} reported in the literature.

Substance/Mineral	$\log_{10}(K_{sp})$
$CaCO_3$ (Calcite) [24]	−8,47
$Ca_{1-x}Mg_x(CO_3)$(Dolomite) [25–29]	~−17 to −19
$Ca(OH)_2$ (CH) [24]	−5,30
$Mg(OH)_2$ [24]	−11,25
$Fe(OH)_3$ [24]	−16,31
$Al(OH)_3$ [23]	−33,52
$CaSO_4 \cdot 2H_2O$[24]	−4,50

The water is a solvent with amphiprotic characteristics, that is, it can act as Brønsted-Lowry acid or Brønsted-Lowry base depending on the solution nature. The ionization constant (K_w) varies with changes in temperature and pressure, and the pK_w value at ambient conditions is approximately 14.0. Another important parameter is the solubility product constant (K_{sp}), can be defined as the relation between the equilibrium of the solid and the aqueous ions in the solution (Eqs. (7) and (8)). The higher the K_{sp}, more soluble is the compound. The K_{sp} values can be calculated using the standard Gibbs free energy of formation ($\Delta_f G^0$) of each species involved at the dissolution at 25 °C (Eq. (9)) [22–24]. The comparison of the values of $\log_{10}(K_{sp})$ for calcareous phases and some phases present in residual cement in the RCA, show significant differences in terms of solubility (Table 1).

$$M_mN_{n(s)} \rightleftharpoons mM^+_{(aq)} + nN^-_{(aq)} \quad (7)$$

$$K_{sp} = [M^+]^m[N^-]^n \quad (8)$$

$$\ln K_{sp} = \frac{\Delta_f G^0}{RT} \quad (9)$$

The higher the $\log_{10}K_{sp}$ values the more soluble the compound is, therefore when comparing the cement CH phase and the phases present in calcareous aggregates, the CH phase is about 1000 times more soluble in water than the calcite and dolomite.

In the literature are reported several studies about the interaction of water with concrete. One of the unusual studies about this phenomenon was developed by Carde, François and Torrenti (1996) [30] and aimed to evaluate the influence of water in concrete containers used to store radioactive wastes. In this study it was observed that the water promotes a chemical attack in the CH and C-S-H phases of the cement paste by partially leaching the calcium, causing the decrease of the compressive strength and increase of the porosity of the concrete. As well as the study reported [29], other studies evidence calcium leaching of the C-S-H and CH phases by water [30–33].

The chemical concepts of K_{sp} and previous studies of calcium leaching in concrete suggest the selective interaction of water with the calcium present in the CH and C-S-H phases, in detriment to the calcium present in the limestones Therefore, the goal of the present study is to establish an innovative method applying the selective dissolution in deionized water for quantifying the cement paste in recycled concrete aggregates containing limestone.

2. Material and methods

2.1. Dissolution tests

The hydrated cement paste (HCP) used in this study was obtained from hydration process (28 days and 0.5 w/c) of commercial Brazilian Cement (CPV), equivalent to Type 1 – ASTM C150. The

materials submitted to the dissolution tests in deionized water were hydrated Portland cement (HCP), quarzitic sand (QS), dolomite (D), calcite (C) and also mixtures between the materials in order to simulate the chemical composition of RCA (Table 2). All materials were powdered by Herzog equipment in a tungsten pan for 2 min in order to improve the mixtures homogenization and also to obtain particle size distribution d_{90} less than 150 μm. The pulverized solids were packed in sealed plastic bags with the intention of avoiding moisture contact and possible carbonation of the hydrated cement.

The dissolution tests were performed with 5.00 g of the materials added to cellulose dialysis sacks with 100 mL of deionized water. The filled dialysis sacks were placed in a container with five liters of deionized water, which was stirred with a magnetic stirrer for 24 h. In the dissolution procedure, pH of the container solution was measured. The tests were performed in 10 days, the deionized water was renewed periodically every day in the container. Supernatants solutions were reserved until the end for ICP-OES analysis and insoluble residues were oven dried at 80 °C until constant mass was obtained.

The membrane used as a filter in the dissolution system is essential for retaining fine particles, as it is commonly used in clays purification and biochemical applications. The dialysis membrane is made of cellulose and is capable of retaining protein particles with molecular weights greater than 12,000 Da. There is no simple conversion unit between Dalton and nanometers, but estimate by equations that the membrane aperture ranges between 1.6 and 10 nm.

The method uses a large amount of water, because each time the water is renewed the chemical equilibrium of the dissolution reaction is shifted to favor the dissolution products. Although it seems a problem to use an immense amount of water, it can be reused after the extraction process in a column with cations exchange resin. The dissolved calcium can also become a by-product to generate calcium carbonate.

2.2. Characterization techniques

Each constituent was characterized before and after the dissolution tests in terms of chemical and mineralogical composition, particle size distribution, thermal decomposition, infrared and Raman spectroscopies; the ions content on the solutions were also analyzed.

The mineralogical composition of each phase was assessed by X-ray powder diffractions (XRD), which patterns were obtained in a Philips – X'Pert PRO PW 3040/00 with Cu source radiation at 45 kV and 50 mA, at range of 2θ from 2 to 70°, step size of 0.02° and 100 s per step for a detailed analysis.

The chemical composition of each phase was obtained by X-ray fluorescence analyzes; the samples were fused with anhydrous lithium tetraborate and obtained the quantitative analysis by comparison with reference materials certified in an X-ray fluorescence spectrometer, PANalytical brand, model Zetium. The water-solubilized ions were analyzed by inductively coupled plasma optical emission spectrometry (ICP-OES) Horiba Jobin Yvon Ultima Expert model.

Table 2
Proportion of the phase mixtures for the simulated RCA samples.

Mixtures	QS (%)	HCP (%)	C (%)	D (%)
1%HCP	84	1	10	5
5%HCP	80	5	10	5
10%HCP	75	10	10	5
20% HCP	65	20	10	5

The analysis of particle size distribution (PSD) was performed by low-angle laser light scattering on the Malvern2000 equipment in Hydro 2000MU sampler. The powder materials were dispersed in isopropyl alcohol, at pump speed 2500 rpm and attenuation of 5–10%.

The thermal analysis were performed in Netzsch, model 490 PC Luxx, coupled with mass spectrometer QMS 403C Aeolos in alumina crucible. The analysis conditions were done with sample mass between 10 and 12 mg, inert atmosphere (N_2 gas) at 50 mL min^{-1}, heating rate of 10 °C min^{-1} at range 30–1200 °C.

The infrared measurements were recorded in BrukerAlpha in the total attenuated reflectance mode in a range of 400–4000 cm^{-1} with spectral resolution of 4 cm^{-1}.

The Raman spectra were recorded in FT-Raman Bruker equipment, model RFS 100/S, with Ge detector (cooled with liquid N_2) and Nd^{3+}/YAG laser (1064 nm), at range of 100–3500 cm^{-1}.

3. Results and discussions

3.1. Dissolution tests: particle size distribution and chemical analysis

One of the important factors that interfere in the dissolution process is the particle size distribution of the solids. Monte Carlo simulation studies demonstrate that the increase of the dissolution rate with the decrease in particle size, and that refer to the kinetic process [31,32]. Based on this concept the samples that were tested by the water dissolution method were pulverized. The particle size distribution (PSD) for the samples tested are shown in Fig. 1. The pulverized materials showed D_{90} values below 150 μm and PSD presented similar results in between the samples. The HCP and QS samples showed a wider PSD compared to the other samples.

The dissolution tests performed for the all samples had pH values checked in the first 15 min and after the 24 h of the initial contact to the deionized water.

The significant increase of the pH value was observed for the samples containing cement paste in its composition, fact associated to the rapid dissolution of the CH phase in an aqueous system. However, for the limestone samples, a gradual increase of the pH values over time was observed (Fig. 2).

The change in pH values for limestone samples indicates slow dissolution, possibly related to kinetic factors and pH value variation of 1.5 and 2.0 for calcite and dolomite, respectively. On samples containing cement paste were observed the quick increase of pH values, it is probably associated with the dissolution of the CH phase. Between the period of 15 and 1440 min the gradual increase of the pH values is observed, a fact possibly related to

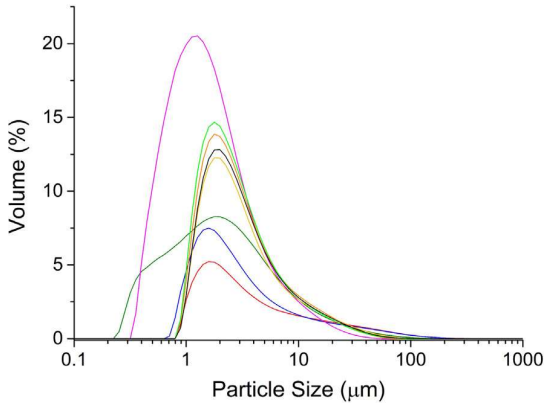

Fig. 1. Particle size distribution of the HCP(–), C(–), D(–), QS(–), 1%HCP(–), 5% HCP (–), 10%HCP (–) and 20%HCP(–) samples.

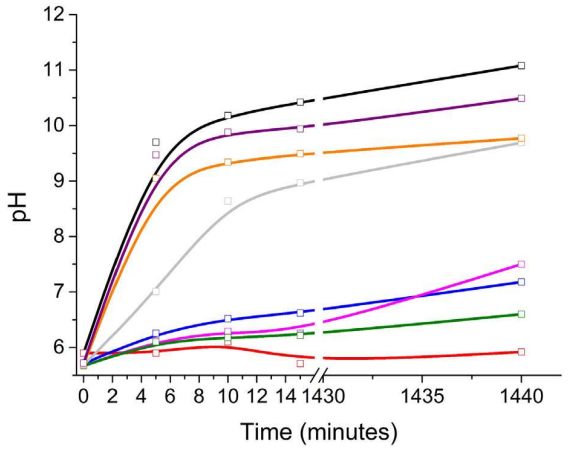

Fig. 2. Solution pH value as function dissolution time for HCP (−□−), QS (−□−), C (−□−), D (−□−), 1%HCP (−□−), 5%HCP (−□−), 10%HCP (−□−) and 20%HCP (−□−).

the secondary reaction of CaO in the C-S-H phase and water, producing $Ca(OH)_2$. The variation of the pH values of the HCP sample after one day of dissolution in water was approximately 5.3 pH units. The variation is much higher when compared to calcareous samples.

In accordance with the pH values obtained at the end of the experiments and the K_{sp} value of the CH phase it was possible to calculate the concentration of calcium ions remaining in the solids, considering the equations (10) and (11). It was established that the final dissolution pH should have values lower than 8.30 for obtain less than 1% of cement paste in the sample.

$$Ca(OH)_{2(s)} \rightleftharpoons Ca^{2+}_{(aq)} + 2\,OH^{-}_{(aq)} \quad (10)$$

$$CaO_{(s)} + H_2O_{(l)} \rightarrow Ca(OH)_{2_{(s)}} \quad (11)$$

At the end of 10 days of dissolution in deionized water and after dry the materials, the residual weights were checked for each one of the samples. The cement paste sample, HCP, present a mass loss of 48%, whereas for the samples of limestone were 9% for dolomite and 4.5% for calcite (Table 3).

The soluble residues obtained after 10 days of dissolution for the samples hydrated cement paste (HCP), quatzitic sand (QS), dolomite (D) and calcite (C) were evaluated by ICP-OES. The results do not show soluble ions for quarzitic sand sample (QS) after the dissolution process. In the samples of calcite and dolomite the partial dissolutions of the phases are observed, however the concentration of soluble residue is about 10 times smaller than the soluble residue of the sample of hydrated cement (see Table 4).

In the soluble residues of HCP, low concentrations of aluminum, silica and sulfur were also found, this could be attributed to the dissolution of phases that present K_{sp} similar to calcium hydroxide, such as phases containing calcium sulphates, for examples, gypsum and ettringite commonly found in RCA. The content of aluminum and silica may also be related to the dissolution of nanometric domain by the dissolution of the calcium oxide of the C-S-H phase with particle size smaller than the opening of the dialysis bag used (d ~ 3.2 nm).

Table 3
Mass loss after the dissolution process.

Samples/mixtures	Mass Remaining (%)	Mass Removed (%)
QS	99.68	0.320
D	91.05	8.950
C	95.52	4.470
HCP	51.97	48.03
1%HCP	99.27	0.730
5%HCP	97.38	2.620
10%HCP	94.46	5.530
20%HCP	89.25	10.75

The chemical composition of the insoluble residue of the HCP sample evidences the enrichment of the Al_2O_3, SiO_2, MgO, Fe_2O_3 content simultaneous to the reduction of the CaO content in 12.4% (Table 5)

The samples QS, C and D do not present significant changes in the chemical composition after the dissolution process. The results of XRF and ICP-OES of the HCP, QS, C and D samples indicate the selectivity of the deionized water in the interaction with the hydrated cement paste.

The simulate RCA samples evidence the correlation between the reduction in calcium content (RCC) and the content of hydrated cement at 1% HCP (RCC = 0.7%), 5% HCP (RCC = 1.0%), 10% HCP (RCC = 1.8%) and 20% HCP (RCC = 4.4%).

3.2. X-ray diffractometry (XRD)

The XRD of the HCP and HCP_H_2O (Fig. 3) corroborate the hypothesis of reducing the content of calcium, after the dissolution process of the hydrated cement (HCP_H_2O) in water; the peaks of the phases CH, ettringite and remaining C_3S of clinker phase are no longer observed. The chemical analysis of the soluble residues corroborates with the analysis of XRD for the sample HCP_H_2O, since show the dissolution of calcium, and also residues of aluminum ions, silica and sulfur.

No changes in the XRD profile after the dissolution process were observed for QS and C samples. The diffraction peaks of dolomite after dissolution became broader and less intense, that could be associated with the decrease in the crystallite size of dolomite sample (Fig. 1A). The XRD profile of simulate RCA samples, 1% HCP, 5%HCP, 10%HCP and 20%HCP do not present significant changes after the dissolution (Fig. 2A), fact attributed to low concentration of the CH phase in the mixtures and high intensity of the peaks of the carbonate phase.

X-ray diffraction is a technique applied for identification and classification of crystalline materials. However, the dissolution process can increase crystal defects in order to favor the formation of phases with low or no crystallinity. In this way it is essential to characterize the solids by techniques that are not directly influenced by the crystallinity of the materials.

3.3. Spectroscopic analyzes: FT-IR and Raman

The analysis of the profile of the infrared spectrum shows shifts and disappearance of bands in the samples D and HCP after the dissolution process, whereas for samples C and QS only changes in band width were observed in the spectra (Figs. 4 and 5). The spectrum will be discussed in three regions: high frequency (>1700 cm^{-1}), mid frequency (ca. 1200-,1600 cm^{-1}) and low frequency (<1200 cm^{-1}). The bands present in the regions of high frequency (>1700 cm^{-1}) are represented by the interactions of the water molecules and carbonate combination bands [33–36]. The FTIR spectrum of the HCP sample shows a broad band at 1648 cm^{-1} assign to water bending vibrations ν_2 (H-O–H) and also two bands at 2800–3700 cm^{-1}, a broadband at 3407 cm^{-1} is attributed to hydrogen bonded (OH-OH) stretching vibration in water molecules, and a band at 3640 relative to the antisymmetric stretching mode ν (OH) of the CH phase [33–36].

The carbonate combination bands, ($\nu_1 + \nu_4$), ($2\ \nu_2 + \nu_4$) e ($2\ \nu_3$) can be observed in the C, C_H_2O, D e D_H_2O spectra at 1800, 2540 e 2870 cm^{-1}, respectively. The spectra of the samples QS, QS_H_2O, C,

Table 4
ICP-OES analysis of soluble residue after dissolution process.

Samples	[C] Ca (mg/L)	[C] Al (mg/L)	[C] Fe (mg/L)	[C] Mg (mg/L)	[C] Na (mg/L)	[C] P (mg/L)	[C] S (mg/L)	[C] Si (mg/L)
C_H_2O	0.92	<LD	<LD	<LD	<LD	<LD	<LD	<LD
D_H_2O	0.89	<LD	<LD	0.91	<LD	<LD	<LD	<LD
QS_H_2O	<LD	<LD	<LD	<LD	<LD	<LD	<LD	<LD
HCP_H_2O	8.62	0.92	<LD	<LD	<LD	<LD	0.44	0.31

Table 5
XRF analysis of insoluble residue before and after dissolution process.

	SiO_2 %	Al_2O_3 %	Fe_2O_3 %	MgO %	CaO %	Na_2O %	K_2O %	P_2O_5 %	LOF %
HCP	15.0	3.4	2.0	1.9	47.1	0.2	0.8	0.20	28.6
HCP_H_2O	24.6	5.5	3.3	3.1	34.7	<0.10	<0.10	0.30	28.1
C	3.1	0.4	0.2	2.1	53.2	<0.10	<0.10	<0.10	41.8
C_H_2O	3.3	0.3	0.1	2.1	52.8	<0.10	<0.10	<0.10	41.9
D	0.6	0.1	0.1	22.0	32.0	<0.10	<0.10	<0.10	46.0
D_H_2O	1.2	0.1	0.1	21.3	31.7	<0.10	<0.10	<0.10	46.2
QS	96.3	1.9	0.1	<0.10	<0.10	<0.10	1.1	<0.10	0.60
QS_H_2O	95.9	2.0	0.1	<0.10	0.2	<0.10	1.1	<0.10	0.80
1%HCP	81.1	1.7	0.2	1.3	7.5	<0.10	1	<0.10	7.9
1%HCP_H_2O	82.0	1.7	0.2	1.3	6.9	<0.10	0.9	<0.10	7.6
5%HCP	79.1	1.8	0.2	1.4	8.7	<0.10	1	<0.10	8.7
5%HCP_H_2O	80.6	1.8	0.3	1.4	7.7	<0.10	0.9	<0.10	8
10%HCP	74.8	1.8	0.3	1.4	10.9	<0.10	1	<0.10	10.2
10%HCP_H_2O	77.7	1.9	0.3	1.5	9.1	<0.10	0.8	<0.10	9.2
20%HCP	66.8	1.9	0.5	1.6	15.4	<0.10	0.9	<0.10	13.5
20%HCP_H_2O	73.2	2.1	0.6	1.7	11	<0.10	0.7	<0.10	11.2

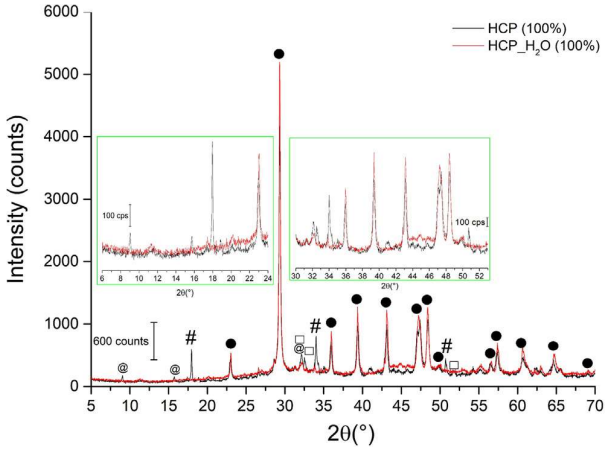

Fig. 3. XRD analysis of HCP and HCP_H_2O samples. *(●) calcite - $CaCO_3$; (□) Hatrurite; (@) Ettringite; (#) $Ca(OH)_2$.

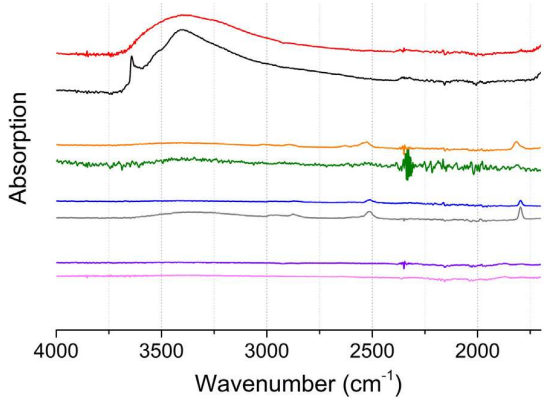

Fig. 4. Infrared spectra at range 4000–1700 cm^{-1} of the samples HCP (-), HCP_H_2O (-), D(-), D_H_2O(-), C(-), C_H_2O(-), QS(-), QS_H_2O(-).

C_H_2O, D and D_H_2O there are no bands related to the stretching and bending vibrations of the water molecules, fact related to the low concentration of water molecules in the limestone and in the QS sample, even after the dissolution process.

The bands present in the mid frequency region of the spectra are related to the antisymmetric stretching of carbonate (ν_3) [34–37]. The respective band are found in the spectra of the samples at D (1471 cm^{-1}), D_H_2O (1417 cm^{-1}), C (1401 cm^{-1}), C_H_2O (1400 cm^{-1}), HCP (1414 cm^{-1}) e HCP_H_2O (1435 cm^{-1}). After the dissolution of dolomite is observed a band shift 1471 cm^{-1} to 1417 cm^{-1}, this is possibly attributed to the decrease in the magnesium content in the sample [34,38].

The region of FTIR in low frequency (<1250 cm^{-1}) are related to bands of silicates, carbonates and sulfates vibrations. The dissolution in deionized water of the HCP sample promotes the disappearance of the broadband at 1113 cm^{-1} assigns to the (S-O) stretching of the sulfate phases, indicating the dissolution of sulfate-containing phases as already suggested by the XRD and ICP-OES analyzes. The bands at 830–890 cm^{-1} e 700–730 cm^{-1} are due to in-plane (ν_4) and out-of-plane (ν_2) bending vibration of CO_3, respectively. The bands at 960, 550 e 440 cm^{-1} are attributed to antisymmetric stretching, bending and deformation vibrations of tetrahedron silicates Si-O [33–35], respectively, these bands can be observed at the spectrum of the sample QS.

The simulate RCA samples spectra did not show significant changes after the dissolution process, this is possibly due to low concentration of hydrated cement. The spectra of the simulate RCA samples can be seen in Fig. 3A and Fig. 4A, available in the supplementary information.

In order to complete the spectroscopic characterization, the FT-Raman analysis was performed. According to Newman et al. (2005) [39], the Raman spectra obtained with near-infrared laser radiation

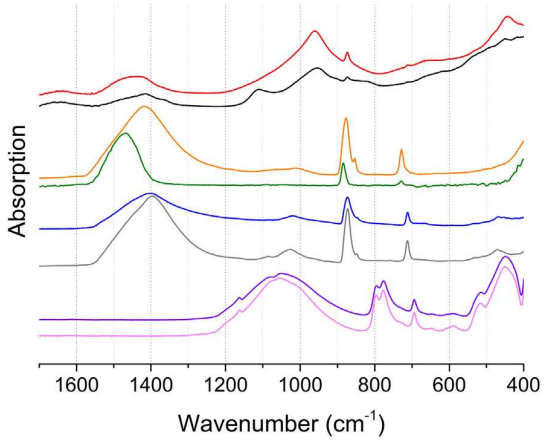

Fig. 5. Infrared spectra at range 1700–400 cm^{-1} of the samples HCP (-), HCP_H_2O (-), D(-), D_H_2O(-), C(-), C_H_2O(-), QS(-), QS_H_2O(-).

show signals in relation to the fluorescence of Portland cement. The FT-Raman analyzes of the HCP sample indicate fluorescence bands at 450, 725, 803, 1027 e 1127 cm^{-1}, after the dissolution process these bands disappear (Fig. 6).

The calcium minerals present particularities in the analysis of Raman spectroscopy when irradiated by laser at 1064 nm (FT-Raman). In the literature studies of calcium minerals in FT-Raman presented unusual bands in the spectrum, such bands have often been misinterpreted as Raman signals, but can be correctly assigned as fluorescence signals, these bands are commonly found in calcium phosphate minerals [40]. Some minerals containing calcium in the composition such as fluorapatite ($Ca_{10}(PO_4)_6F_2$) [41], calcium hydroxide ($Ca(OH)_2$)[40,42] and hydroxyapatites ($Ca_{10}(PO_4)_6OH_2$) [43] show fluorescence profile in the FT-Raman spectrum. The bands of hydrated cement, clinker and calcium minerals present similarities in the signal profile and position of the fluorescence bands (Table 6) [39–43].

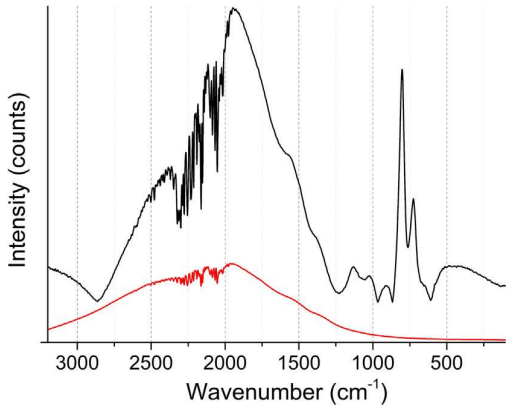

Fig. 6. Raman analysis of HCP (-) and HCP_H_2O (-) samples by laser excitation at 1064 nm.

The clinker phases C_3S and C_2S also present fluorescence signals in FT-Raman analysis, however the CS (Wollastonite ($CaSiO_3$)) phase does not have fluorescence profile [39]. There is no clear explanation for this fluorescence, but Newman et al. (2005) [39], suggest the association of fluorescence signal with the structural disorder provided by orthosilicates compounds presents in the C-S-H, during the cement polymerization the intensity of fluorescence signal decrease due to the rearrangement of silicates groups in the structure. The evidences of fluorescence signals in clinker phases (C_3S and C_2S) and hydrated cement paste (C-S-H), lead to associate these fluorescence signals in FT-Raman to those found in some calcium minerals as calcium hydroxide, fluorapatite and hydroxyapatites.

Some authors suggest that cement fluorescence signals are associated with transition elements or rare earths [40,41]. Manganese oxide (MnO_4^{3-}), for example, shows a similar luminescence profile of hydrated cement [44]. In the present work as evidenced in XRF analysis, there is no manganese oxide in the HCP sample.

The calcium hydroxide, however, has similar luminescence signals and can be one of the factors responsible for luminescence signals in hydrated cement, however, this hypothesis does not explain the fluorescence signals found in C_3S and C_2S clinker phases [39].

In the study related to the fluorescence bands of hydroxyapatites replaced with lead ($Ca_{10-x}Pb_x(PO_4)_6(OH)_2$), Hadrich, Lautié e Mhiri (2001) [43] take note of fluorescence bands at 690 and 769 cm^{-1} in FT-Raman analysis when $x \leq 7$, and suggest that could be attributed to the orientation and disorder of the anions (OH^-) associated with the divalent cations (M^{2+}) especially where there is calcium in the composition. The hypothesis suggested by the authors is plausible to explain the FT-Raman spectrum of hydrated cement phases. The Ca^{+2} ions are associated to hydroxyls in both the C_2S, C_3S, C-S-H and CH phases, so the fluorescence bands observed in FT-Raman analysis are possibly associated with structural factors of the phases. Thereby, the disappearance of the fluorescence bands in the FT-Raman spectrum after dissolution could be assigned to the reduction or complete extraction of calcium ions associated with hydroxyl, present in CH and C-S-H. In case of the suggested hypothesis could be confirmed, Raman spectroscopy could be used as an important qualitative tool to identify the absences of the CH, C_2S, C_3S and C-S-H phases in the cement. Future applications may involve the classification of the CDW or evaluate the viability of the extraction of the hydrated cement in the processing.

The Raman spectrum of the simulated mixtures before and after the dissolution process are presented in the supplementary information (Fig. 5A).

Table 6
Literature Raman data for clinker, cement and calcium minerals phases.

HCP[a] (cm^{-1})	$Ca(OH)_2$[b,c] (cm^{-1})	Hydroxiapatite[c] (cm^{-1})	C_3S[d] (cm^{-1})	C_2S[d] (cm^{-1})	Cement[d] (cm^{-1})
450					
			570		
725	721–723	690		730	650
803	776–800	770		805	800
915	920		940		
1027				1100	1000
1127		1155			1130

a-Present work b-Ref. [42] c-Ref. [40] d-Ref. [39].

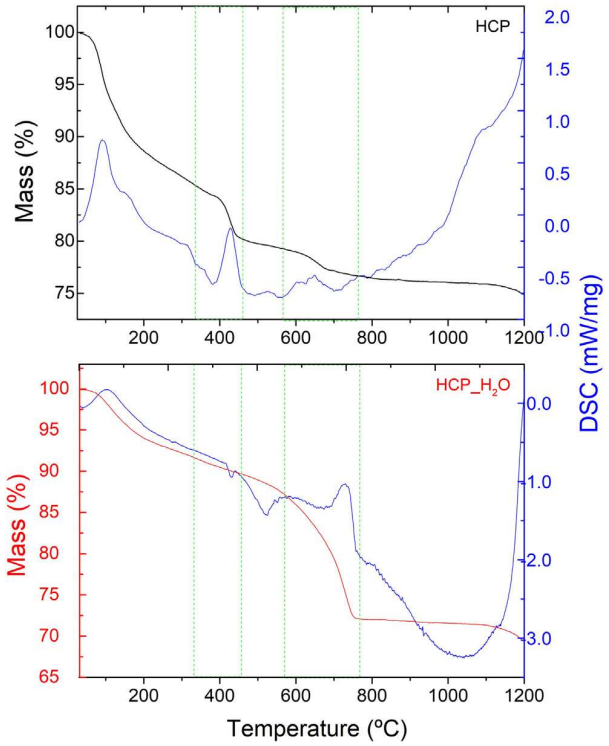

Fig. 7. TG/DSC analysis of HCP and HCP_H_2O samples.

3.4. Thermal analysis coupled with mass spectrometer (MS)

The thermal analysis of HCP and HCP_H_2O shows differences in TG/DSC profile after dissolution process. In Fig. 7, the main differences between the HCP and HCP_H_2O are indicated by green boxes.

The thermal decomposition of the HCP sample can be divided into four stages of mass loss by the TG curves:

a) The first stage of mass loss between 33 and 200 °C, is associated with losses of hydration and constitution water in hydrated cements, confirmed by typical endothermic process observed on DSC curve (Fig. 7) and fragment *m*/*z* 18 (H_2O) presented in the MS curve (Fig. 8) [45,46]. After the dissolution process, the decrease in the amount of water is observed about 3.6% (Table 7).

b) The second step of mass loss between 350 and 500 °C is also associated with water loss, a fact corroborated by *m*/*z* 18.0 (H_2O) in the MS curve. This decomposition step is related to dehydroxylation process of the CH phase [5,46–49]. As evidenced after the dissolution process, this step is no longer observed, the mass loss value on this step decrease by 2.8% in HCP_H_2O sample (Table 7).

c) The third stage of mass loss is associated with the carbonate thermal decomposition [5,46–48]. The TG curve of the HCP sample shows a defined mass loss event at 500–800 °C, with an endothermic peak at DSC curve and fragment *m*/*z* 44 (CO_2). The mass losses on this step could be relate with the calcium carbonate thermal decomposition equilibrium in order to calculate the content of $CaCO_3$ in the samples. The HCP sample presented 7.5% $CaCO_3$ residue, whereas after the dissolution process in the HCP_H_2O sample it was observed that increase in $CaCO_3$ content (38.5%), it is due to the reaction between calcium ions released during the dissolution process and carbonate generated by the reaction between water and gaseous CO_2 in the environment. The remaining CaO from carbonate thermal decomposition represent 29,9% in mass. Comparing the results obtained by the TG calculations and XRF analysis, it was verified the

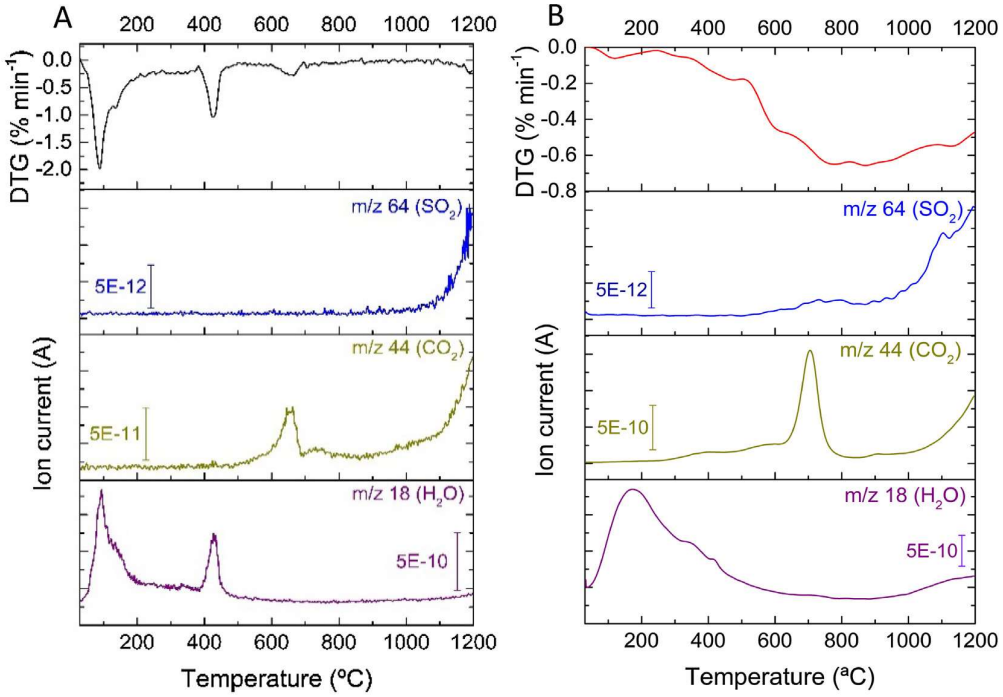

Fig. 8. Mass spectrometry analysis of HCP (A) and HCP_H_2O (B) samples coupled with TG analysis, the fragments found in thermal decomposition process, *m*/*Z* 18 (H_2O), 44 (CO_2) and 64 (SO_2).

Table 7
Mass loss of TG decomposition events for standards samples HCP, HCP_H_2O, QS, QS_H_2O, C, C_H_2O, D, D_H_2O.

Samples	1° Step		2° Step		3° Step		4° Step	
	Mass loss (%)	Temp. Range (°C)	Mass loss (%)	Temp. range (°C)	Mass loss (%)	Temp. range (°C)	Mass loss (%)	Temp. range (°C)
HCP	11.38	30–200	5.24	430–500	3.29	500–800	1.56	800–1200
HCP_H_2O	7.78	30–200	2.41	430–500	16.94	500–800	2.60	800–1200
QS	1.32	35–1200	–	–	–	–	–	–
QS_H_2O	1.96	35–1200	–	–	–	–	–	–
C	1.90	100–500	40.55	500–850	0.43	850–1200	–	–
C_H_2O	0.42	100–500	31.63	500–850	0.65	850–1200	–	–
D	1.53	35–300	47.12	365–800	3.00	800–1200	–	–
D_H_2O	1.15	35–300	46.32	365–800	0.75	800–1200		

difference of 4.8%, that can probably represent the calcium sulphate and/or cement hydrates phases that were not dissolved in the process.

d) The fourth stage of mass loss is attributed to the decomposition of sulfates as indicated by the presence of the fragment m/z 64 (SO_2) in MS curve [50]. After the dissolution process, the sulfate content increases by 1.0%. The process of dissolution promotes an increasing in the sulfate content by 1.0%, probably due to free sulfates present as contaminant in the dialysis sacks.

The TG/DSC/MS analyzes of the dolomite, calcite and quartzitic sand samples showed no changes in the thermal decomposition profile after the dissolution process as observed in Table 7 and Fig. 9.

At the end of the sample's characterization by thermal analysis of the HCP sample it was possible to verify that despite 10 days of the dissolution process in deionized water, it was not possible to remove 100% of the calcium present in hydrated cement paste, however, the TG calculations indicated only about 5.0% CaO corresponding to the undissolved phases. It's necessary to consider also the problems resulting of $CaO/Ca(OH)_2$ to $CaCO_3$ conversion, that consequently generates an increase of molar mass.

Although with the premise that in 10 days of dissolution the simulate RCA samples follow the same behavior of the sample containing 100% HCP it was possible to establish a simple equation in order to relate the experimental and real cement content. The assumptions concepts applied to satisfy the equation were: the kinetic and thermodynamic factors of the hydrated cement dissolution in deionized water are independent of the composition of simulate RCA samples; the influences of the carbonate and other

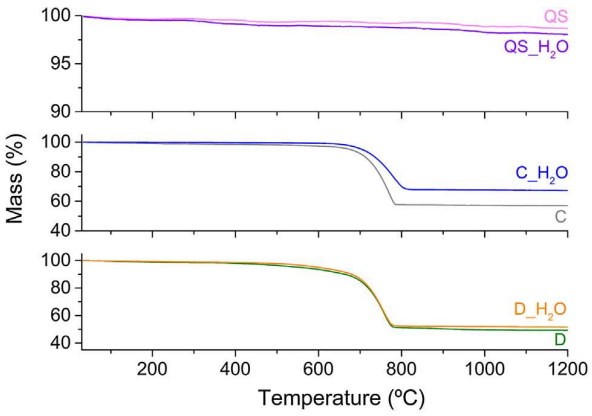

Fig. 9. TG analysis of calcite (C), dolomite (D) and quartzitic sand (QS) before and after dissolution process (H_2O).

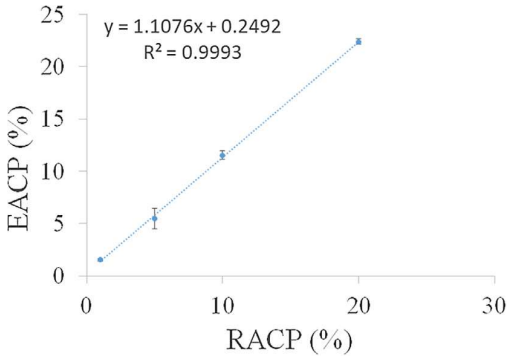

Fig. 10. Relation between estimated amount of cement paste (EACP) and real amount of cement paste (RACP).

phases dissolution and the conversion of $CaO/Ca(OH)_2$ to $CaCO_3$ were not considered in the equation.

A good correlation between the experimental results of experimental (EAPC) and real (RAPC) contents of cement paste in simulate RCA were found (Fig. 10).

$$\%\,Cement\ paste\ content = \frac{removed\ mass\ sample(\%) \times 100}{removed\ mass\ HCP(\%)} \quad (12)$$

The equation represents successfully the content of cement paste on RCA simulated samples by dissolution method in deionized water. The dissolution method in water presents good precision and accuracy, although it overestimates the content of cement paste, this is probably due to the partial leaching of the limestone and ettringite phases.

4. Conclusions

The method presents good efficiency in the removal of the calcium ions from the hydrated cement phases, C-S-H and CH. The selectivity of the hydrated cement reaction with water was confirmed by the characterization techniques. The chemical analyzes of XRF of HCP_H_2O sample indicate the enrichment of SiO_2, Al_2O_3, Fe_2O_3, MgO and P_2O_5 phases, this is mostly due to the dissolution of calcium ions as indicated by ICP-OES analysis. No enrichment process occurs in calcite, dolomite and quarzitic sand samples.

The applied method was able to remove the CH and ettringite phases from hydrated cement as indicated by XRD analysis. There are no significant changes in the XRD profiles of calcite, dolomite and quarzitic sand samples after dissolution.

The FTIR spectroscopic analysis indicates the disappearance of the CH phase on HCP_H_2O sample corroborating the XRD analysis. The Raman spectra of the HCP sample presents fluorescence bands as described in the literature, however after the dissolution process

these bands disappeared. The fluorescence profile observed in FT-Raman analysis for clinker and hydrated cement has not been clarified yet, however the hypothesis that best explains the disappearance of the bands after the dissolution process relates luminescence to structural factors between calcium and hydroxyl ions presents in C-S-H and CH phases.

The dissolution method in deionized water presents good analytical results for quantifying the cement paste content in recycled concrete aggregates containing limestone, however, more studies are necessary to improve the method in order to minimize the carbonate contamination and to reduce the time of dissolution.

Declaration of Competing Interest

None.

Acknowledgements

The authors are grateful for the undergraduate students, Lais Bento Cazellato and Ana Yumi Jacomo whose annual activity reports were important for the development of this study. The authors are gratefully acknowledge CNPq-CAPES for the financial support (process 88881 068109 2014-01) and scholarship (process 88887.125222/2015-00), the Technological Characterization Laboratory (LCT) and the Lamellar Solids Laboratory (LaSol) (FAPESP, 2011/50318-1) and Molecular Spectroscopy Laboratory (LEM) from University of São Paulo. The information and views set out in this study are those of the authors and do not necessarily reflect the opinion of the founding agencies.

Appendix A. Supplementary data

Supplementary data to this article can be found online at https://doi.org/10.1016/j.conbuildmat.2019.116875.

References

[1] Z. Wu, A.T.W. Yu, L. Shen, G. Liu, Quantifying construction and demolition waste: An analytical review, Waste Manag. 34 (2014) 1683–1692, https://doi.org/10.1016/j.wasman.2014.05.010.
[2] R.V. Silva, J. De Brito, R.K. Dhir, Properties and composition of recycled aggregates from construction and demolition waste suitable for concrete production, Constr. Build. Mater. 65 (2014) 201–217, https://doi.org/10.1016/j.conbuildmat.2014.04.117.
[3] M. Behera, S.K. Bhattacharyya, A.K. Minocha, R. Deoliya, S. Maiti, Recycled aggregate from C&D waste & its use in concrete - A breakthrough towards sustainability in construction sector: A review, Constr. Build. Mater. 68 (2014) 501–516, https://doi.org/10.1016/j.conbuildmat.2014.07.003.
[4] S.C. Angulo, A. Mueller, Determination of construction and demolition recycled aggregates composition, in considering their heterogeneity, Mater. Struct. Constr. 42 (2009) 739–748, https://doi.org/10.1617/s11527-008-9417-3.
[5] Z. Zhao, S. Remond, D. Damidot, W. Xu, Influence of hardened cement paste content on the water absorption of fine recycled concrete aggregates, J. Sustain. Cem. Mater. 2 (2013) 186–203, https://doi.org/10.1080/21650373.2013.812942.
[6] H.F.W. Taylor, Cement chemistry, second ed., Thomas Telford Publishing, London, 1997.
[7] C. Fang, J. Xie, B. Zhang, B. Yuan, C. Wang, Impact properties of geopolymeric concrete: A state-of-the-art review, IOP Conf. Ser. Mater. Sci. Eng. 284 (2018) 1–5, https://doi.org/10.1088/1757-899X/284/1/012012.
[8] M. Alexander, S. Mindess, Aggregates in Concrete, First, Taylor & Francis, New York, 2005.
[9] S. Mindess, J.F. Young, D. Darwin, Concrete, second ed., Prentice Hall, Upper Saddle River, 2002.
[10] J.F. Young, W. Hansen, Volume relationships for CSH formation based on hydration stoichiometries, MRS Proc. 85 (1987) 313–322, https://doi.org/10.1557/PROC-85-313.
[11] A.N. Christensen, T.R. Jensen, J.C. Hanson, Formation of ettringite, Ca(6)Al(2)(SO4) 3(OH)(12)·26H2O, AFt, and monosulfate, Ca(4)Al(2)O(6)(SO4)·14H 2O, AFm-14, in hydrothermal hydration of Portland cement and of calcium aluminum oxide - Calcium sulfate dihydrate mixtures studied by in situ synchrot, J. Solid State Chem. 177 (2004) 1944–1951, https://doi.org/10.1016/j.jssc.2003.12.030.
[12] R.V. Silva, J. de Brito, R.K. Dhir, Availability and processing of recycled aggregates within the construction and demolition supply chain: A review, J. Clean. Prod. 143 (2017) 598–614, https://doi.org/10.1016/j.jclepro.2016.12.070.
[13] P. Belin, G. Habert, M. Thiery, N. Roussel, Cement paste content and water absorption of recycled concrete coarse aggregates, 2014. doi:10.1617/s11527-013-0128-z.
[14] ASTM C-127, Specific Gravity and Absorption of Coarse Aggregate, 2001, 1–5.
[15] ASTM C128-15, Standard Test Method for Relative Density (Specific Gravity) and Absorption of Fine Aggregate, 2015, 1–6.
[16] A. Barbudo, F. Agrela, J. Ayuso, J.R. Jiménez, C.S. Poon, Statistical analysis of recycled aggregates derived from different sources for sub-base applications, Constr. Build. Mater. 28 (2012) 129–138, https://doi.org/10.1016/j.conbuildmat.2011.07.035.
[17] M. Quattrone, B. Cazacliu, S.C. Angulo, E. Hamard, A. Cothenet, Measuring the water absorption of recycled aggregates, what is the best practice for concrete production?, Constr Build. Mater. 123 (2016) 690–703, https://doi.org/10.1016/j.conbuildmat.2016.07.019.
[18] A. Abbas, G. Fathifazl, B. Fournier, O.B. Isgor, R. Zavadil, A.G. Razaqpur, S. Foo, Quantification of the residual mortar content in recycled concrete aggregates by image analysis, Mater. Charact. 60 (2009) 716–728, https://doi.org/10.1016/j.matchar.2009.01.010.
[19] S. Braymand, S. Roux, H. Fares, K. Déodonne, F. Feugeas, Separation and quantification of attached mortar in recycled concrete aggregates, Waste Biomass Valoriz. 8 (2017) 1393–1407, https://doi.org/10.1007/s12649-016-9771-2.
[20] M.S. de Juan, P.A. Gutiérrez, Study on the influence of attached mortar content on the properties of recycled concrete aggregate, Constr. Build. Mater. 23 (2009) 872–877, https://doi.org/10.1016/j.conbuildmat.2008.04.012.
[21] J.I. Alvarez, A. Martín, P.J. García Casado, I. Navarro, A. Zornoza, Methodology and validation of a hot hydrochloric acid attack for the characterization of ancient mortars, Cem. Concr. Res. 29 (1999) 1061–1065, https://doi.org/10.1016/S0008-8846(99)00090-3.
[22] T.L. Brown, H.E. LeMay, B.E. Bursten, J.R. Burdge, Chemistry: The Central Science, nineth ed.,., Pearson Education, 2005.
[23] D.A. Skoog, D.M. West, F.J. Holler, S.R. Crouch, Fundamentals of Analytical Chemistry, eighth ed., CENGACE Learning, São Paulo, 2006.
[24] W.M. Haynes, D.R. Lide, T.J. Bruno, Handbook of Chemistry and Physics, 97th ed., CRC PRESS, Boca Raton, 2017.
[25] K.J. Hsu, Chemistry of dolomite formation, in: G. V. Chilingar, H.J. Bissell, R.W. Fairbridge (Eds.), Dev. Sedimentol. 9B, Elsevier Ltd, amsterdam, 1967: pp. 169–192.
[26] P. Bénézeth, U.N. Berninger, N. Bovet, J. Schott, E.H. Oelkers, Experimental determination of the solubility product of dolomite at 50–253 °C, Geochim. Cosmochim. Acta. 224 (2018) 262–275, https://doi.org/10.1016/j.gca.2018.01.016.
[27] L.A. Sherman, P. Barak, Solubility and dissolution kinetics of dolomite in Ca-Mg-HCO3/CO3 solutions at 25°C and 0.1 MPa carbon dioxide, Soil Sci. Soc. Am. J. 64 (2000) 1959–1968.
[28] D. Langmuir, Stability of carbonates in the system MgO-CO2-H20, J. Geol. 73 (1965) 730–754.
[29] R.M. Garrels, M.E. Thompson, R. Siever, Stability of some carbonates At 25-degrees-C and one atmosphere total pressure, Am. J. Sci. 258 (1960) 402–418, https://doi.org/10.2475/ajs.258.6.402.
[30] C. Carde, R. François, J.M. Torrenti, Leaching of both calcium hydroxide and C-S-H from cement paste: Modeling the mechanical behavior, Cem. Concr. Res. 26 (1996) 1257–1268, https://doi.org/10.1016/0008-8846(96)00095-6.
[31] L. Briese, R.S. Arvidson, A. Luttge, The effect of crystal size variation on the rate of dissolution – A kinetic Monte Carlo study, Geochim. Cosmochim. Acta. 212 (2017) 167–175, https://doi.org/10.1016/j.gca.2017.06.010.
[32] G. Wang, D.S. Xu, N. Ma, N. Zhou, E.J. Payton, R. Yang, M.J. Mills, Y. Wang, Simulation study of effects of initial particle size distribution on dissolution, Acta Mater. 57 (2009) 316–325, https://doi.org/10.1016/j.actamat.2008.09.010.
[33] P. Yu, R.J. Kirkpatrick, B. Poe, P.F. McMillan, X. Cong, Structure of Calcium Silicate Hydrate (C-S-H): Near-, Mid-, and Far-Infrared Spectroscopy, J. Am. Ceram. Soc. 82 (2004) 742–748, https://doi.org/10.1111/j.1151-2916.1999.tb01826.x.
[34] B.J. Zhan, D.X. Xuan, C.S. Poon, C.J. Shi, S.C. Kou, Characterization of C-S-H formed in coupled CO2–water cured Portland cement pastes, Mater. Struct. Constr. 51 (2018), https://doi.org/10.1617/s11527-018-1211-2.
[35] M.Y.A. Mollah, W. Yu, R. Schennach, D.L. Cocke, A Fourier transform infrared spectroscopic investigation of the early hydration of Portland cement and the influence of sodium lignosulfonate, Cem. Concr. Res. 30 (2000) 267–273, https://doi.org/10.1016/S0008-8846(99)00243-4.
[36] S.N. Ghosh, S.K. Handoo, Infrared and Raman spectral studies in cement and concrete (review), Cem. Concr. Res. 10 (1980) 771–782, https://doi.org/10.1016/0008-8846(80)90005-8.
[37] S. Gunasekaran, G. Anbalagan, S. Pandi, Raman and infrared spectra of carbonates of calcite structure, J. Raman Spectrosc. 37 (2006) 892–899, https://doi.org/10.1002/jrs.1518.
[38] M.E. Böttcher, P.-L. Gehlken, D.F. Steele, Characterization of inorganic and biogenic magnesian calcites by Fourier Transform infrared spectroscopy, Solid State Ionics. 101–103 (1997) 1379–1385, https://doi.org/10.1016/S0167-2738(97)00235-X.

[39] S.P. Newman, S.J. Clifford, P.V. Coveney, V. Gupta, J.D. Blanchard, F. Serafin, D. Ben-Amotz, S. Diamond, Anomalous fluorescence in near-infrared Raman spectroscopy of cementitious materials, Cem. Concr. Res. 35 (2005) 1620–1628, https://doi.org/10.1016/j.cemconres.2004.10.001.
[40] A. Aminzadeh, Fluorescence bands in the FT-Raman spectra of some calcium minerals, Spectrochim. Acta - Part A Mol. Biomol. Spectrosc. 53 (1997) 693–697, https://doi.org/10.1016/S1386-1425(96)01848-3.
[41] E.L. Varetti, E.J. Baran, Raman or fluorescence spectra? About the use of FT-raman techniques on inorganic compounds, Appl. Spectrosc. 48 (8) (1994) 1028–1029, https://doi.org/10.1366/0003702944029613.
[42] T.Y. Kwon, T. Fujishima, Y. Imai, FT-Raman spectroscopy of calcium hydroxide medicament in root canals, Int. Endod. J. 37 (2004) 489–493, https://doi.org/10.1111/j.1365-2591.2004.00831.x.
[43] A. Hadrich, A. Lautié, T. Mhiri, Vibrational study and fluorescence bands in the FT-Raman spectra of Ca10-xPbx(PO4)6(OH)2compounds, Spectrochim., Acta - Part A Mol. Biomol Spectrosc. 57 (2001) 1673–1681, https://doi.org/10.1016/S1386-1425(01)00402-4.
[44] U. Oetliker, M. Herren, H.U. Güdel, U. Kesper, C. Albrecht, D. Reinen, Luminescence properties of Mn^{5+} in a variety of host lattices: Effects of chemical and structural variation, J. Chem. Phys. 100 (1994) 8656–8665, https://doi.org/10.1063/1.466720.
[45] I. Pane, W. Hansen, Investigation of blended cement hydration by isothermal calorimetry and thermal analysis, Cem. Concr. Res. 35 (2005) 1155–1164, https://doi.org/10.1016/j.cemconres.2004.10.027.
[46] L. Alarcon-Ruiz, G. Platret, E. Massieu, A. Ehrlacher, The use of thermal analysis in assessing the effect of temperature on a cement paste, Cem. Concr. Res. 35 (2005) 609–613, https://doi.org/10.1016/j.cemconres.2004.06.015.
[47] P. Mounanga, A. Khelidj, A. Loukili, V. Baroghel-Bouny, Predicting Ca(OH)2 content and chemical shrinkage of hydrating cement pastes using analytical approach, Cem. Concr. Res. 34 (2004) 255–265, https://doi.org/10.1016/j.cemconres.2003.07.006.
[48] J. Dweck, P. Mauricio, A. Carlos, V. Coelho, F.K. Cartledge, P.M. Buchler, A.C.V. Coelho, F.K. Cartledge, P. Mauricio, A. Carlos, V. Coelho, F.K. Cartledge, P.M. Buchler, A.C.V. Coelho, F.K. Cartledge, Hydration of a Portland cement blended with calcium carbonate, Thermochim. Acta 346 (2000) 105–113, https://doi.org/10.1016/S0040-6031(99)00369-X.
[49] R. Trauchessec, J.M. Mechling, A. Lecomte, A. Roux, B. Le Rolland, Hydration of ordinary Portland cement and calcium sulfoaluminate cement blends, Cem. Concr. Compos. 56 (2015) 106–114, https://doi.org/10.1016/j.cemconcomp.2014.11.005.
[50] L. Ma, P. Ning, S. Zheng, X. Niu, Reaction mechanism and kinetic analysis of the decomposition of phosphogypsum via a solid-state reaction, Ind. Eng. Chem. Res. 49 (2010) 3597–3602, https://doi.org/10.1021/ie901950y.